reinforcement ratio of the RC model was equivalent to the SC model (Figure 2). The dowel rebars were extended all the way up to the height of the wall, and the depth of the anchor length inside the foundation was same as in the SC wall pier specimens.

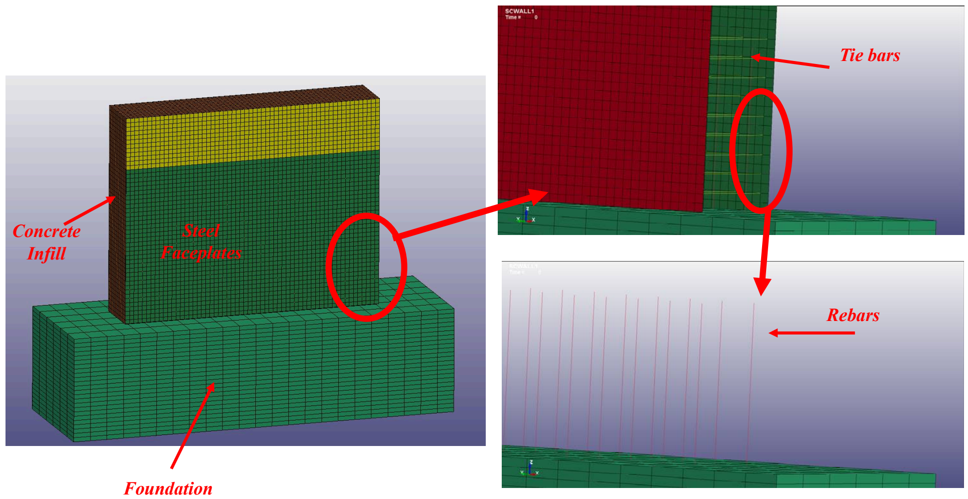

Figure 4. Finite element model details developed for Specimen#1

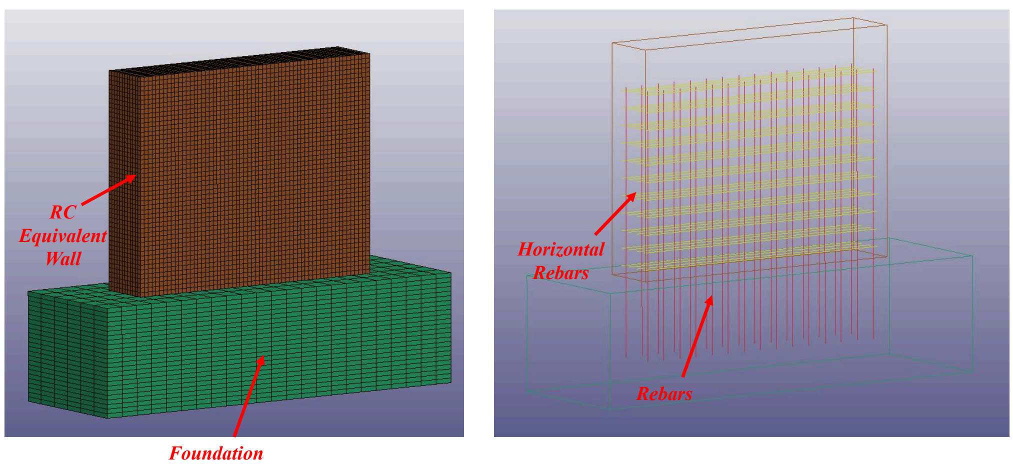

Figure 5. Details of the equivalent RC model developed in LS-Dyna

Figure 6 shows the lateral load-drift ratio comparison of the Specimen#1 and its equivalent RC model under monotonic loading. The walls do not reach their expected lateral load capacities obtained from moment-curvature analysis. They both undergo sliding shear failure. FEMs for Specimen#1 predicted the failure of the extreme tension dowel rebar (vertical reinforcement) to occur at 450 kips. The dowel rebar exceeds 15% plastic strain at this load level.

Figure 7 show the lateral load-drift comparison for Specimen#2 and its equivalent RC model. The Specimen#2 FEM lateral load capacity matches Vn-RC. The FEM capacity exceeds

Vn-318. However, extreme dowel rebar under tension reaches 15% plastic strain at 650 kips lateral force. Sliding shear failure is expected for this specimen in the test.

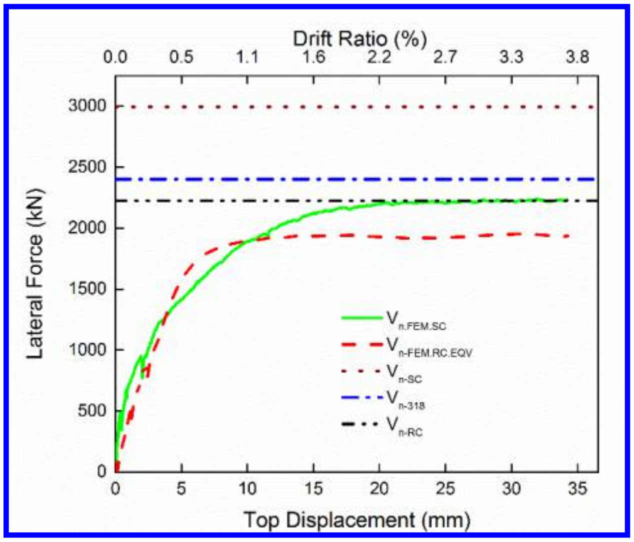

Figure 6. Lateral load-drift comparison for Specimen #1 and equivalent RC wall

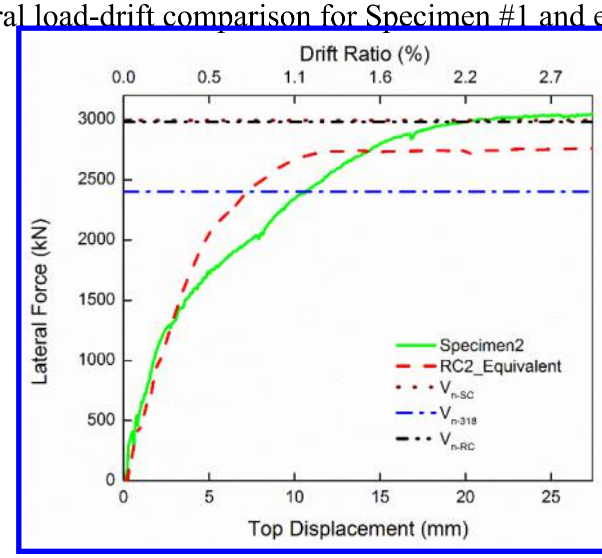

Figure 7. Lateral load-drift comparison for Specimen #2 and equivalent RC wall

Test Results (Overstrength connection)

The specimens were tested under load reversals. Force-displacement history of the first specimen along with comparisons with FEM results are shown here. Figure 8 shows the cyclic response of Specimen#1. The expected in-plane lateral load capacity of the specimen was around 2300 kN as shown in Table 3. The expected lateral load capacity was based on the sectional analysis of the wall cross section. The specimen experienced base shear of around 2200 kN at a drift ratio of 1.2%. The failure of the specimen occurred when the longitudinal reinforcement rebars failed at drift ratio of 4%. Figure 9 shows the comparison of the FEM results with the test backbone curve. The initial stiffness of the SC wall, RC equivalent wall, and tested wall are very similar to each other.

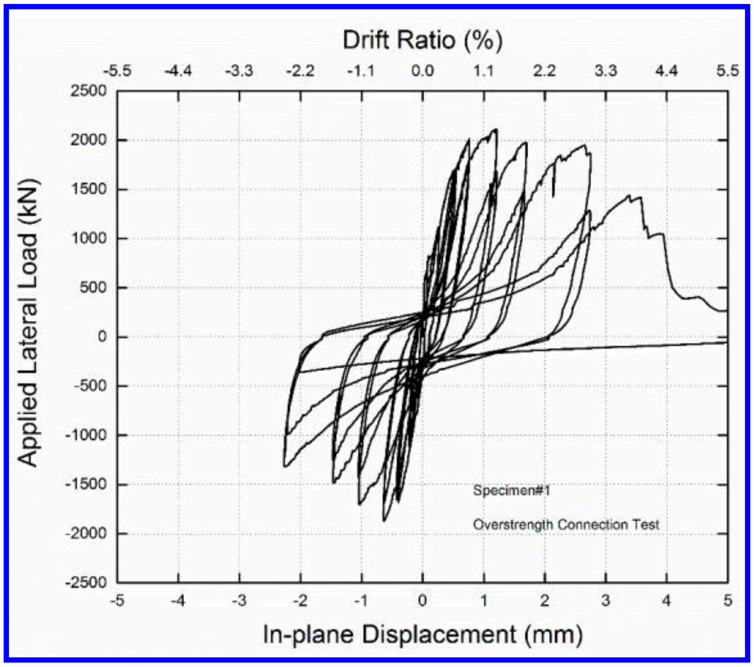

Figure 8. Cyclic response of Specimen#1 (overstrength-connection)

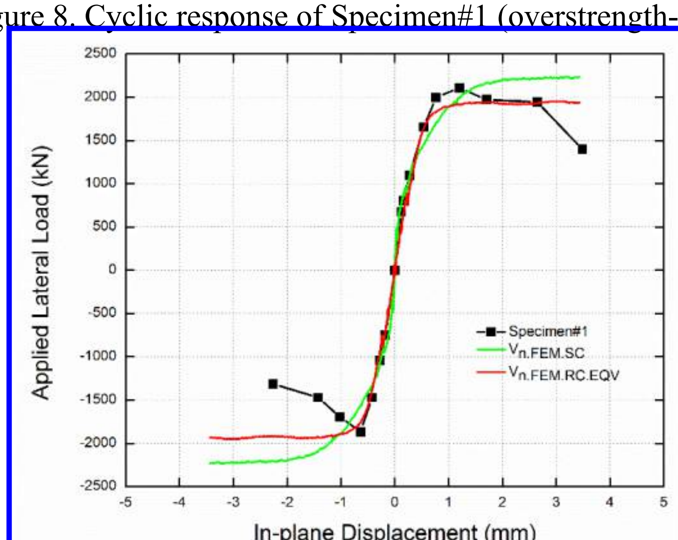

Figure 9. Comparison of test backbone curve with FEM results.

CONCLUSIONS

This paper discussed two different anchoring options for SC wall piers and their design. Full strength connection provided enough anchor strength for the SC walls to reach to their in-plane capacity. The specimens failed under flexure even with very small aspect ratios. The failure mechanism was rupture of the faceplates under tension and crushing of the concrete infill under compression.

The flexural capacity of the RC portion of the specimens for overstrength connection specimens was calculated by moment-curvature analysis. ACI 318 limitations,Vn-318, and shear friction capacity, Vn-sfl, for Specimen#1 were greater than the flexural capacity of the specimen, Vn-RC. ACI upper limit for the individual wall pier strength, Vn-318, was lesser than the shear-friction, Vn-sf, and flexural capacity, Vn-RC, of Specimen#2. Although the first specimen was theoretically a flexure dominated wall, both specimens are expected to fail in shear. The connector elements (shear studs and tie bars) inside the specimens were detailed to prevent premature buckling of the steel faceplates.

The test results show that the Specimen#1 of overstrength connection specimens reached to its RC flexural capacity. 3D finite element models of the designed specimens were developed in LS-Dyna. Results of the FEMs were compared with the test results, and they were in good agreement.

REFERENCES

ACI 318 (2008), "Building Code Requirements for Structural Concrete and Commentary" American Concrete Institute, Farmington Hills, MI

American Institute for Steel Construction (AISC) (2010). "Specification for Structural Steel Buildings", Chicago, Illinois, USA.

AISC (2014). "Specification for Safety-Related Steel Structures for Nuclear Facilities" AISC N690s1, public review draft, dated May 1, 2014, AISC, Chicago, IL.

American Society of Civil Engineers (ASCE) (2010). "Minimum Design Loads for Buildings and Other Structures." ASCE 7-10. Reston, VA: ASCE.

Bruhl, J., and Varma, A.H. (2015). "Missile Impact Behavior and Design of Composite SC Walls." International Journal of Impact Engineering, Elsevier Science, Vol. 75, pp. 75-87, http://dx.doi.org/10.1016/j.ijimpeng.2014.07.015, 1st Tier.

Kurt, E.G., Varma, A.H., Booth, P.N., and Whittaker, A. (2013). "SC Wall Piers and Basemat Connections: Numerical Investigation of Behavior and Design." Transactions of the 22nd International Conference on Structural Mechanics in Reactor Technology (SMiRT 22), IASMIRT,CA, USA. http://engineering.purdue.edu/~ahvarma/Publications/Pap_872_ver_3.pdf

U.S. Department of Energy. Accident analysis for aircraft crash into hazardous facilities (DOE-STD-3014). Washington, D.C.: U.S. Department of Energy;

Bruhl, J., and Varma, A.H. (2015). "Missile Impact Behavior and Design of Composite SC Walls." International Journal of Impact Engineering, Elsevier Science, Vol. 75, pp. 75-87, http://dx.doi.org/10.1016/j.ijimpeng.2014.07.015, 1st Tier.

Kurt, E.G., Varma A.H., Epackachi S., and Whittaker A.S. (2015). "Rectangular SC Wall Piers: Seismic Behavior and Design." ASCE Structures Congress, Portland, Oregon, USA.

Varma, A.H., Zhang, K., Chi, H., Booth, P. and Baker, T. (2011). "In-plane shear behavior of SC composite walls: theory vs. experiment." Proceedings of the 21st IASMiRT Conference (SMiRT 21), New Delhi, India, Paper ID #764.

Zhang, K., Varma, A.H., Malushte, S., and Gallocher, S. (2014). "Effects of Shear Connectors on the Local Buckling and Composite Action in Steel Concrete Composite Walls." Nuclear Engineering and Design, Special Issue on SMiRT-21 Conference, Vol. 269, pp. 231-239, Elsevier Science.http://dx.doi.org/10.1016/j.nucengdes.2013.08.035

Rehabilitation of Reinforced Concrete Structures Using Shape Memory Alloys

Sherif M. Daghash[1] and Osman E. Ozbulut[2]

[1]Dept. of Civil and Environmental Engineering, Univ. of Virginia, P.O. Box 400742, Charlottesville, VA 22904-1000. E-mail:smd7an@virginia.edu
[2]Dept. of Civil and Environmental Engineering, Univ. of Virginia, P.O. Box 400742, Charlottesville, VA 22904-1000. E-mail: ozbulut@virginia.edu

Abstract

The near-surface-mounted (NSM) strengthening method is a relatively new method for rehabilitation of reinforced concrete structures and can overcome some of the disadvantages of the other strengthening systems. In NSM method, longitudinal grooves are first cut into the concrete cover of an RC member, then reinforcing bars or strips, are inserted in these grooves and bonded with an epoxy paste or cementitious material. Although the NSM reinforcement can preclude delamination-type failure, one of the main factors that affect the efficiency of the NSM method is still the bond between the NSM reinforcement and the concrete. Shape memory alloys (SMA) are a class of metallic alloys that can remember their original shape upon being deformed. Besides their ability to recover large strains with minimal residual deformations, SMAs possess excellent corrosion resistance, good energy dissipation capacity, and high fatigue properties. This study investigates bond characteristics and load transfer mechanisms between NSM SMA reinforcement and concrete. A modified pullout test set-up that consists of a C-shaped concrete block, where the NSM reinforcement are placed at the center of gravity of the block, are used for experimental investigations. The effects of various parameters such as NSM reinforcement type, embedment length, type of epoxy on the bond behavior are studied. The slip of the SMA reinforcement relative to concrete is measured using DIC method at the loaded and free ends of the specimen and the bond-slip curves are developed.

INTRODUCTION

Over their service life, reinforced concrete (RC) structures need to be strengthened due to different factors (Huang et al. 2010). Traditional methods used to strengthen concrete structures include but are not limited to steel plate bonding, steel jacketing, precast concrete jacketing, and external prestressing. These techniques have drawbacks such as susceptibility to corrosion damage, need for intensive labor and detailing, and increase in the dimensions and weight of structural members

(Hollaway and Teng 2008). Fiber reinforced polymers (FRPs) have been widely considered to restore stiffness and strength of concrete structures due to their favorable properties such as high corrosion resistance, lightweight and high tensile strength (Teng et al. 2002). FRPs have been mostly used as an externally bonded (EB) system, where sheets of FRPs are bonded to external surface of concrete, for strengthening existing concrete structures. However, premature debonding failure was observed in the EB systems by many researchers (Seracino et al. 2007; Liu et al. 2006; Bonacci and Maalej 2001; Bizindavyi and Neale 1999). The EB systems may also be subjected to fire, vandalism and vehicle impact. The near-surface-mounted (NSM) strengthening method is a relatively new technology and becoming an attractive method, which can overcome some of the disadvantages of the EB systems (Ceroni et al. 2012). In NSM method, longitudinal grooves are first cut into the concrete cover of an RC member, then reinforcing bars or strips, are inserted in these grooves and bonded with an epoxy paste or cementitious material.

Although the NSM reinforcement can preclude delamination-type failure, one of the main factors that affect the efficiency of the NSM method is still the bond between the NSM reinforcement and the concrete (Soliman et al. 2011). Previous studies indicated that FRP rods and laminates could not achieve full material strength due to bond and anchorage problems (Sharaky et al. 2013). An active strengthening technique where the NSM reinforcement is prestressed can lead to better utilization of the material and enhance the serviceability by reducing the crack size/extent and service load deflections. Yet, the studies on the prestressed NSM applications have been limited to laboratory investigations because it is very difficult to prestress the NSM reinforcement (Casadei et al. 2006; Hajihashemi et al. 2011; Gaafar 2007). Furthermore, it is noted that the ductility and deformability of the concrete members strengthened with prestressed NSM FRP are reduced with the increasing prestress level due to the linear elastic behavior of the FRPs (Nordin and Täljsten 2006).

Shape memory alloys are a class of metallic alloys that can remember their original shape upon being deformed. This shape recovery ability is due to reversible phase transformations between different solid phases of the material. The phase transformation can be mechanically induced (superelastic effect) or thermally induced (shape memory effect). Besides their ability to recover large strains with minimal residual deformations, SMAs possess excellent corrosion resistance, good energy dissipation capacity, and high fatigue properties (Ozbulut et al. 2011). Due to their excellent properties, the SMAs have been considered in a wide range of applications in civil engineering (Andrawes and DesRoches 2005; Ozbulut and Hurlebaus 2011a-b, 2012a-b; Zhu and Zhang 2007; Yang et al. 2010; Saiidi and Wang 2006).

SMA bars can also be used for active and passive NSM strengthening of RC structures. The passive NSM with superelastic SMAs will enable enhanced bond performance without the need for any special mechanical anchorages due to the hooked ends of the SMA bars, improved post-event functionality due to re-centering capability of SMAs, and improved impact load response. The active NSM technique with shape memory effect SMAs will eliminate the need for the jacking equipment; enable field implementation of prestressed NSM strengthening technique; enable adjusting the pre-stress level as needed during the service life of structure; and provide larger load carrying capacity, flexural stiffness, deformation capacity, and ductility. This study explores the bond characteristics of NSM SMA bars by conducting modified pullout tests adapted to near-surface mounted reinforcement.

EXPERIMENTAL METHODS

Specimen Preparation and Test Matrix

To investigate the bond behavior of NSM SMA reinforcement, the C-shaped concrete block specimens with a groove at the center of the block for embedment of the NSM reinforcement were prepared as shown in Figure 1. The foams with different geometry were placed inside the formwork to form the required grooves and spaces before the concrete was cast. The dimensions and shape of the 12-in concrete block were chosen to eliminate the influence of the specimen size on the test failure mode and to maintain the stability of the cube and eliminate any eccentricity during testing. This modified pullout specimen for NSM reinforcement also allow the test to be performed in a slip-control mode and provide visual access to the testing zone compared with other beam pullout test setups (De Lorenzis et al. 2002). The 28-day compressive strength of concrete was around 5500 psi.

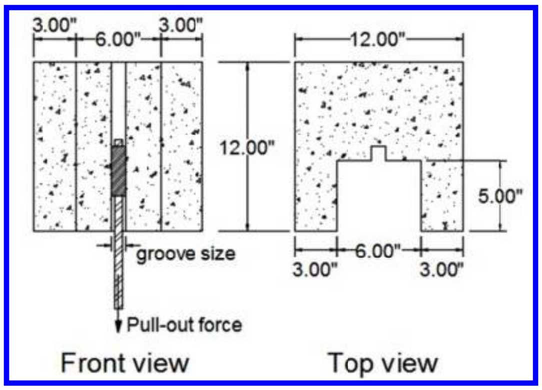

(a)

(b)

Figure 1. (a) Dimensions of the concrete block, (b) foam placed inside the formwork to form the spaces and grooves.

The test was performed in two stages. In the first stage, three types of epoxy were used to bond six ½-in. sandblasted SMA bars to concrete, and bond tests were carried out to specify the strongest epoxy to be used in the following stage. The three epoxies were Sikadur® 30 (*S30)* Hi-modulus, Sikadur® 32 (*S32)* Hi-modulus, and BASF® MasterEmaco ADH 1490 (*ADH1490*). In this stage, the bond length was 7 times the bar diameter ($7d_b$) with a square groove with side dimension twice the diameter of the used bar (1x1 inches). As it will be discussed later, the *S32* epoxy was reported to have the strongest bond in the first stage. Therefore, it was used to prepare all the specimens of the second stage. In the second stage, the effects of changing the embedment length, surface condition, and SMA bar diameter on the bond between the NSM reinforcement and concrete were studied. Three embedment lengths were considered: $5d_b$, $7d_b$ and $12d_b$. The surface of the SMA bars was modified by epoxy coating or sandblasting. Two bar diameters of 5/8 in. and 3/4 in. were also considered in the test matrix. In all the specimens, the square groove dimension was twice the bar diameter. The total SMA bar length was 12 in. A length of 1.5 in. was left from the edge of the concrete block to the start of epoxy application to prevent edge the block shear failure of concrete, and 0.5 in. of the SMA bar was left as a free at the unloaded end. Two specimens were tested for each test parameter.

Additionally, two specimens were prepared using 1/3-in. diameter sandblasted hooked-end SMA bars to study the effect of adding end hook on the bond strength. In the first specimen, only the hooked part was bonded to the concrete, while in the second specimen the bonded part included the hook plus $7d_b$ length of the straight bar. Table 1 summarizes the test matrix.

Table 1. Pullout test matrix.

Number of specimens	Bar diameter (in.)	Surface	Embedded Length	Epoxy type
2	1/2	Sandblasted	$7d_b$	*S30*
2	1/2	Sandblasted	$7d_b$	*S32*
2	1/2	Sandblasted	$7d_b$	*ADH 1490*
2	1/2	Sandblasted	$5d_b$	*S32*
2	1/2	Sandblasted	$12d_b$	*S32*
2	1/2	Epoxy coated	$7d_b$	*S32*
1	5/8	Sandblasted	$7d_b$	*S32*
1	3/4	Sandblasted	$7d_b$	*S32*
1	1/3 with hook	Sandblasted	End hook only	*S32*
1	1/3 with hook	Sandblasted	End hook plus $7d_b$	*S32*

Test Procedure

The pullout tests were performed after 7 days from applying the epoxy to bond the NSM reinforcement to concrete. The tests were conducted on a 55-kip MTS® servo hydraulic machine. A special steel cage was prepared to hold the specimens in the machine and perform the test. During testing, SMA bars were pulled out of the epoxy-filled grooves inside the concrete blocks in a displacement-controlled manner with a rate of 0.0072 in./min. The loads were recorded using the MTS data acquisition system. Digital Image Correlation (DIC) system, provided by Correlated Solution, Inc., was used to measure displacements and strains of the SMA bar, epoxy, and concrete. To this end, a non-periodic, isotropic, and high contrast speckle surface pattern of black dots on white background was applied on the specimens to assure accurate measurements from the DIC system with the lowest possible noise (Reedlunn et al. 2013). The DIC system conducts the measurements of displacement and strain by recording the deformation history of the speckle surface pattern using a fast-rate camera to capture a series of pictures then analyzing the data using commercial software. Therefore, the accuracy of those measurements depends mainly on the quality of the surface pattern. Figure 2 shows the pull-out test setup and the concrete block test specimen.

Figure 2. Pullout test setup.

RESULTS AND DISCUSSIONS

In this section, the results of the pull-out tests for each specimen were reported and discussed in terms of failure load (P_f), failure mode, average bond stress at SMA bar-epoxy interface (τ_{avg1}), average bond stress at epoxy-concrete interface (τ_{avg2}), SMA bar slip at the loaded end (S_1) and at the free end (S_2) (Sharaky et al. 2013). The average bond stresses at both bar-epoxy and epoxy-concrete interfaces were calculated using the following equations:

$$\tau_{avg1} = \frac{P_f}{\pi d_b l_b}$$

$$\tau_{avg2} = \frac{P_f}{3b\, l_b}$$

where b is the groove side dimension, l_b is the embedment length, and $3bl_b$ represents the perimeter of epoxy-concrete interface. Table 2 summarizes the results for each test specimen.

Design Factors and Failure Modes

Epoxy Type

In the first stage of the test, three epoxy types were used to prepare six specimens and pull-out tests were conducted. The objectives of that stage were to observe the effects of epoxy type on the bond behavior between concrete and NSM reinforcement, and to determine the strongest epoxy to be used for the next stage. Figure 3 represents the average bond stress-slip curves of the loaded end of the bar for the three tested epoxies. It can be observed that the bond-slip curves always start with linear elastic portions, which represent the initial resistance of the bonded bar to the pull-out tension force through the bond between the bar and epoxy. The bond between the bars and epoxy depends mainly on two factors to transfer load: (i) the mechanical interlock between the bar and the epoxy and (ii) the adhesion occurring by the surface friction between the bar and the epoxy.

Table 2: Failure loads, average bond stresses, and slips of test specimens.

First stage (1/2 inch sandblasted SMA bar, bond length is $7d_b$)						
Specimen ID	P_f (Ib)	τ_{avg1} (psi)	τ_{avg2} (psi)	S_1 (in)	S_2 (in)	Failure mode
ADH1490-1	6091	1108	580	0.067	0.056	Bar slippage
ADH1490-2	5804	1056	553	0.072	0.051	Bar slippage
S30-1	8169	1486	778	0.197	0.190	Bar slippage
S30-2	8471	1541	807	0.085	0.074	Bar slippage
S32-1	11167	2031	1064	0.157	0.122	Bar-epoxy failure
S32-2	10525	1914	1002	0.143	0.068	Bar-epoxy failure
Second stage (Used epoxy was *S32* Hi-modulus)						
Specimen ID	P_f (Ib)	τ_{avg1} (psi)	τ_{avg2} (psi)	S_1 (in)	S_2 (in)	Failure mode
$5d_b$-1	7299	1859	973	0.0845	0.077	Concrete splitting
$5d_b$-2	7695	1960	1026	0.085	0.078	Concrete splitting and epoxy damage
$12d_b$-1	11184	1187	621	0.118	0.08	Bar slippage
$12d_b$-2	11894	1262	661	0.107	0.088	Bar slippage
Epoxy coated-1	10919	1986	1040	0.130	0.119	Bar-epoxy failure
Epoxy coated-2	10823	1969	1031	0.121	0.107	Bar slippage
5/8 inches bar	11851	1380	660	0.117	0.110	Concrete and epoxy splitting
3/4 inches bar	11832	957	501	0.130	0.043	Bar-epoxy failure
Hooked only bar	3386	-	-	0.235	-	Bar slippage
Hooked bar $+7d_b$	4398	-	-	0.249	-	Bar slippage